Physica B 459 (2015) 79–87

Contents lists available at ScienceDirect

Physica B

journal homepage: www.elsevier.com/locate/physb

Effect of ZnO on spectroscopic properties of Sm^{3+} doped zinc phosphate glasses

M. Seshadri [a,b], M. Radha [a,b], D. Rajesh [a], L.C. Barbosa [b], C.M.B. Cordeiro [b], Y.C. Ratnakaram [a,*]

[a] Department of Physics, Sri Venkateswara University – SVU, Tirupati 517502, India
[b] Instituto de Física Gleb Wataghin, Univiversidade Estadual de Campinas – UNICAMP, Campinas 13083-970, Brazil

ARTICLE INFO

Article history:
Received 9 July 2014
Received in revised form
24 October 2014
Accepted 8 November 2014
Available online 20 November 2014

Keywords:
Sm^{3+}
Phosphate glass
Judd
Ofelt analysis
Emission cross-sections

ABSTRACT

Spectroscopic properties of Sm^{3+} containing zinc oxide based phosphate glasses in the chemical composition $(50-x)P_2O_5+20Na_2HPO_4+9AlF_3+xZnO+1Sm_2O_3$ (where $x=5$, 10, 15, 20 and 25) have been studied. Raman, optical absorption, emission spectra and luminescence decay profiles were recorded and systematically analyzed. Using Judd–Ofelt theory, Judd–Ofelt intensity parameters Ω_λ ($\lambda=2$, 4 and 6), spontaneous radiative transition probabilities (A_{rad}), radiative lifetimes (τ_R), branching ratios (β) were calculated and discussed. With 400 nm wavelength excitation, the emission spectra and decay lifetime of $^4G_{52}$ level of Sm^{3+} doped zinc-phosphate glasses were studied. The branching ratios and emission cross-sections for the transition, $^4G_{5/2}\rightarrow{}^6H_{7/2}$ are found to be higher for $x=25$ mol% of zinc-phosphate glass matrix. The observed decay profiles were found to be exhibiting non-exponential behavior for all zinc-phosphate glasses, due to non-radiative energy transfer among the excited Sm^{3+} ions.

1. Introduction

Spectroscopic investigations of rare earth (RE^{3+}) doped optical glasses are important to develop optoelectronic devices such as solid state lasers, optical amplifiers, phosphors, solar cells [1–5]. Spectral properties of rare earth ions in glasses vary in a wide range depending on chemical composition of glass formers and modifiers. Phosphate glass possesses a large glass formation region and is a good host for fluorescent ions. Since the first theoretical treatment of sensitized luminescence for the electric dipole transition by Forster [6], the energy transfer (ET) phenomenon has been studied extensively in phosphate based inorganic phosphors, crystals and glasses [7,8]. The presence of ZnO as modifier imparts additional mechanical strength, chemical durability, besides lowering thermal expansion coefficient, hygroscopic nature and also found to be attractive due to its good optical, electrical and magnetic properties. Addition of AlF_3 in the form of intermediate enhances rare earth luminescence and lifetime by reusing non-radiative losses. Among rare earth ions, trivalent samarium (Sm^{3+}) is widely considered as one of the best active luminescent ion. It exhibits a strong orange–red fluorescence in the visible region. The very large number of energy levels lying close to each other renders the interpretation of the absorption spectra rather cumbersome. Sm^{3+} ions emitting $^4G_{5/2}$ level in the visible region exhibit relatively high quantum efficiency and different quenching channels. Especially, Sm^{3+} doped glasses have stimulated extensive interest due to their potential applications for color displays, visible solid state lasers, photodynamic therapy (PDT) light sources and high density optical memory devices [9–12]. Moreover, Sm^{3+} can be easily reduced into Sm^{2+} under reducing atmosphere [13], ionizing radiation [14] or femtosecond laser irradiation [15] and are particularly interesting for persistent spectral hole burning (PSHB) studies [16]. Based on optical absorption and emission bands of intra-configurational f–f transitions, the energy level intensities of Sm^{3+} ions in several host media were described and estimated quantitatively by using the Judd–Ofelt (J–O) theory [17,18].

Recently, spectroscopic and radiative properties of Sm^{3+} doped K–Mg–Al phosphate glasses were reported by Srinivasa Rao et al. [19]. Judd–Ofelt parameters and radiative properties of Sm^{3+} ions doped zinc bismuth borate glasses were studied by Agarwal et al. [20]. Seshadri et al. [21] had reported the spectroscopic and laser properties of Sm^{3+} ions doped in different phosphate glasses. Caldino et al. [22] had studied optical spectroscopy and waveguide fabrication in Sm^{3+}/Tb^{3+} doped zinc–sodium–aluminosilicate glasses. Luminescence, structural and dielectric properties of Sm^{3+} doped impurities in strontium lithium bismuth borate glasses were reported by Rajesh et al. [23].

In the present paper, the authors report the optical absorption and luminescence properties and decay process of Sm^{3+} doped zinc phosphate glasses. The Judd–Ofelt intensity parameters (Ω_2,

* Corresponding author. Fax: +55 19 3521 5428.
E-mail addresses: seshumeruva@gmail.com, drmeruva@ifi.unicamp.br (M. Seshadri), ratnakaramyc@gmail.com (Y.C. Ratnakaram).

http://dx.doi.org/10.1016/j.physb.2014.11.016
0921-4526/

Ω_4 and Ω_6), radiative transition probabilities (A_{rad}), radiative lifetimes (τ) and branching ratios (β) were estimated from the absorption spectra using Judd–Ofelt analysis. Derived from the multichannel radiative transition of Sm^{3+}, the visible emission peaks at 560 nm, 597 nm, 649 nm and 702 nm were observed. The stimulated emission cross-sections (σ_P) of the observed emission peaks were estimated and the fluorescence decay lifetime measurements were reported.

2. Experimental

The zinc-phosphate glasses studied in the present work are based on the composition $(50–x)P_2O_5+20Na_2HPO_4+xZnO+9AlF_3+1Sm_2O_3$ (where $x=5$, 10, 15, 20 and 25 mol%). All the samples were prepared from the starting chemical constituents $NH_4H_2PO_4$, Na_2HPO_4, $ZnCO_3$, AlF_3 and Sm_2O_3. About 10 g batch of glass composition in each case was mixed in an agate mortar and melted in electric furnace at 850 °C for 1 h in porcelain crucible. The melt was quenched to room temperature in a brass plate. The obtained glass samples were subsequently annealed at 300 °C for 3 h and then cooled down slowly to room temperature.

The densities of the glass samples were determined using Archimedes principle with water as the immersion liquid for all the zinc-phosphate glasses. The refractive indices of the glasses were measured on an Abbe refractometer using 1-bromonaphtalene as an adhesive coating. Raman spectra were measured using Lab Raman HR 800 Confocal Raman spectrometer. Optical absorption spectra were recorded on JASCO V-570 UV–vis–NIR spectrophotometer in the wavelength region 300–1800 nm. Emission spectra of Sm^{3+} doped glasses were measured using SPEX Fluorolog-2 fluorometer (Model-II) under the excitation wavelength, 400 nm using Xe arc lamp as the excitation source in the wavelength region 500–750 nm. The fluorescence decay lifetime measurements were also carried under the excitation wavelength 400 nm for Sm^{3+} doped zinc phosphate glasses. All these measurements carried out at room temperature.

3. Results and discussion

3.1. Physical properties and optical band gaps

Table 1 gives some of the physical properties of the Sm^{3+} doped zinc-phosphate glasses which are calculated from the fundamental properties like densities, refractive indices and average molecular weights of the glasses. It is observed that the density of the present glass systems decreases with increase in ZnO content,

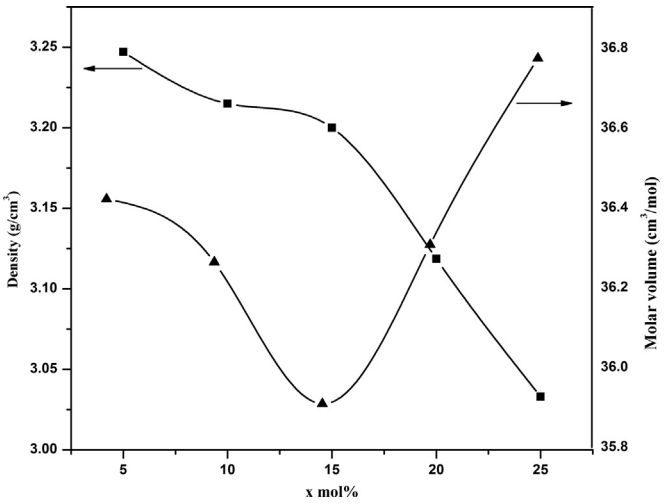

Fig. 1. Variation of density and molar volume with x (mol%) in Sm^{3+} doped zinc-phosphate glasses.

while the molar volume decreased for $x=5$–15 mol% and increased for $x=20$–25 mol% of ZnO phosphate glasses. The variation of density and molar volume with x in zinc-phosphate glasses is shown in Fig. 1. It is also interested to notice that the ionic radius, r_i (Å) and inter-ionic distance, r_p (Å) decreased for $x=5$–15 mol% and increased for $x=20$–25 mol% of ZnO phosphate glasses.

Davis and Mott [24] obtained optical band gaps (E_{opt}) for both direct and indirect transitions at the fundamental absorption edge of crystalline or non-crystalline materials using the following formula:

$$\alpha(\varpi) = \frac{B\left(\hbar\varpi - E_{opt}\right)^n}{\hbar\varpi} \quad (1)$$

where $\alpha(\omega)$ is the absorption coefficient, B is a constant, $\hbar\omega$ is the photon energy of the incident radiation, E_{opt} is the optical band gap and n is an index which can assume values 1, 2, 3, 1/2 or 3/2 depending on the nature of the inter-band electronic transitions. The above equation with $n=2$ agrees well for chalcogenide and oxide glasses [25]. For direct transitions $n=1/2$ and for indirect transitions $n=2$. Optical band gap values are obtained both for indirect and direct transitions of Sm^{3+} doped zinc-phosphate glass from the variation of $(\alpha\hbar\omega)^{1/2}$ with $\hbar\omega$ and from the variation of $(\alpha\hbar\omega)^2$ with $\hbar\omega$ graphs respectively. The respective values of E_{opt} are obtained by extrapolating to $(\alpha\hbar\omega)^2=0$ for direct transitions and $(\alpha\hbar\omega)^{1/2}=0$ for indirect transitions. It is observed that the optical band gaps for indirect transitions are presented in

Table 1
Certain physical properties of Sm^{3+} doped zinc-phosphate glasses.

Physical properties	$x=5$ mol%	$x=10$ mol%	$x=15$ mol%	$x=20$ mol%	$x=25$ mol%
Molar mass, M (g mol^{-1})	118.3	116.6	114.9	113.2	111.5
Density, d (g/cm^3)	3.25	3.21	3.20	3.12	3.03
Refractive index, n_d	1.652	1.652	1.650	1.652	1.652
Molar refractivity, R_M (cm^{-3})	13.317	13.259	13.098	13.275	13.446
Molar volume, V (cm^3/mol)	36.4	36.2	35.9	36.3	36.8
Dielectric constant, $\in$	2.729	2.729	2.722	2.729	2.729
Electronic polarizability, $\alpha_e \times 10^{24}$ (cm^3)	5.28	5.26	5.19	5.26	5.33
Concentration, $N \times 10^{-22}$ (ions per/cm^3)	1.654	1.661	1.678	1.659	1.638
Ionic radius, r_i (Å)	1.581	1.579	1.574	1.580	1.586
Inter-ionic distance, r_p (Å)	3.925	3.919	3.906	3.921	3.937
Field strength, $F \times 10^{-16}$ (cm^2)	1.199	1.203	1.211	1.202	1.192
Reflection losses, R (%)	6.044	6.044	6.016	6.044	6.044
Indirect band gap, E_{opt} (eV)	3.96	3.95	3.92	3.92	3.90
Direct band gap, E_{opt} (eV)	3.96	3.95	3.93	3.91	3.88

Table 1. From the table, it is observed that the optical band gaps for both indirect and direct transitions are nearly equal for all zinc-phosphate glasses. The optical band gaps for both indirect and direct transitions decreases with the increase of ZnO content (x mol%) could be explained using the concept of additivity of local gaps [26] and similar results observed for the other rare earth doped host glasses [27,28].

Generally, in the case of phosphate glasses, the absorption edge is attributed to the optically induced transition of the electrons between oxygen 2p orbital and non-occupied phosphorus 3d orbital. The charged non-bridging oxygen (NBO) of the PO_4 unit would introduce 2p energy levels, which are higher than those of the bridging oxygen (BO). The higher 2p energy levels of the NBO will lower the energy required to induce the transition of electrons to the non-occupied phosphorus 3d orbital, and lead to the lower E_{opt} of the glasses [29]. Moreover, the increased hydroxyl content in the phosphate glass may shifts the cutoff towards the longer wavelength side due to increased concentration of NBO in phosphate glasses [30]. Therefore, in the present work, decreased energy bandgap with the increased ZnO content in phosphate glass matrix is due to the decreased phosphate chain length and relative content of bridging oxygen (BO), respectively.

3.2. XRD and Raman spectra

The X-ray diffraction profiles (not shown) of the Sm^{3+} doped zinc-phosphate glasses exhibits completely amorphous with no diffraction peaks. The Raman spectra of the zinc-phosphate glasses are shown in Fig. 2. Raman spectroscopy is employed to study the structure of phosphate glasses and the band assignments which are reported in literature [31–33]. In the present work, the Raman bands between 200 and 600 cm^{-1} is due to the bending vibrations of orthophosphate units. The band at 360 cm^{-1} is due to the bending vibrations of the phosphate polyhedral and at 557 cm^{-1} may be attributed to the symmetric stretch of PO^- bonds. The band observed between 600 and 800 cm^{-1} is due to the symmetric stretching of the bridging P–O bond. Its shifts from lower frequency (699 cm^{-1}) to higher frequency (752 cm^{-1}) for $x=10$–25 mol% of ZnO in phosphate glass matrix. This might be explained by the increase of P–O bond length or by the change in the chain P–O–P bond angles as an effect of the modifiers on the network structure. The bands between 1050 and 1210 cm^{-1} are related to the symmetric stretching mode of non-bridging $(PO_2)_{sym}$ representing the Q^2 units and the bands shifted from higher frequency (1188 cm^{-1}) to lower frequency (1054 cm^{-1}) with the increase of ZnO (x in mol%) in phosphate glass matrix. At $x=25$ mol% of zinc-phosphate glass matrix, another peak at 1219 cm^{-1} is also an indicative of Q^2 units within the glass structure [31]. It is also observed that the intensities of the Raman bands are increased at $x=10$ mol% and then decreased for $x=15$, 20 and 25 mol% of ZnO in phosphate glass matrices.

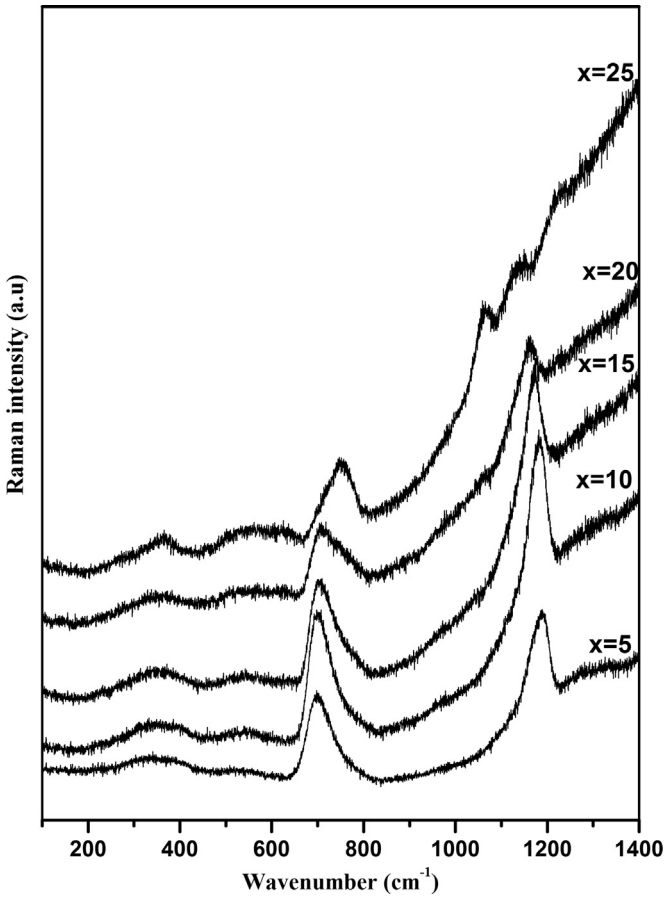

Fig. 2. Raman spectra of Sm^{3+} doped zinc-phosphate glasses.

3.3. Absorption spectra and Judd–Ofelt analysis

Fig. 3 shows the optical absorption spectra of Sm^{3+} doped zinc-phosphate glasses in the 300–1800 nm spectral region. Nineteen bands are observed and located at 316, 339, 343, 360, 373, 401, 415, 439, 476, 526, 581, 943, 1076, 1229, 1378, 1486, 1544 and 1585 nm. These are associated with the transitions from the ground state $^6H_{5/2}$ to the excited states $^4P_{3/2}$, $^4H_{11/2}$, $^4D_{7/2}$, $^4D_{3/2}$, $^4D_{1/2}+{}^6P_{7/2}$, $^6P_{3/2}$, $^6P_{5/2}$, $^4G_{5/2}$, $^4I_{11/2}+{}^4H_{3/2}+{}^4M_{15/2}$, $^4F_{3/2}$, $^4G_{5/2}$, $^6H_{11/2}$, $^6F_{9/2}$, $^6F_{7/2}$, $^6F_{5/2}$, $^6F_{3/2}$, $^6F_{1/2}$ and $^6H_{15/2}$. There is no change in the position of the absorption peak and spectral profile of each transition for zinc-phosphate glasses are similar to those in other Sm^{3+} doped glasses for f–f transitions and are not easily affected by surrounding ions. The spectral intensities of the absorption bands are estimated by measuring the areas under the absorption curves using the formula

$$f_{\exp} = 4.32 \times 10^{-9} \int \varepsilon(\nu) d\nu \quad (2)$$

where $\int \varepsilon(\nu) d\nu$ represents the area under the absorption curve the molar absorptivity $\varepsilon(\nu)$ of the corresponding band at energy ν (cm^{-1}) under the integral is given by $\varepsilon(\nu)=A/cl$, where A is the absorbance, c is the concentration of the lanthanide ion in mol/l and l is optical path length. The magnetic dipole contributions are negligible and hence they are not considered in the present work. The theoretical oscillator strengths, f_{cal}, of the electric dipole transitions, within the f^N, configurations can be calculated using Judd–Ofelt theory [17,18]. The three Judd–Ofelt intensity parameters Ω_λ ($\lambda=2$, 4 and 6), were calculated by fitting the electric dipole contributions of experimental and calculated spectral intensities [34].

Table 2 shows the experimental, calculated spectral intensities and Judd–Ofelt intensity parameters of Sm^{3+} doped zinc-phosphate glasses. The Judd–Ofelt intensity parameters in the present work are compared with other glasses and are presented in the table. It is observed that the spectral intensities are found to be higher at $x=25$ mol% of zinc-phosphate glass indicating higher crystal field asymmetry and lower at $x=5$ mol% of zinc-phosphate glass indicating lower crystal field asymmetry. As referred previously by many authors [19–23,35,36], Ω_2 parameter is an indicator of the covalency of lanthanide sites, Ω_4 and Ω_6 parameters are related to the bulk property and rigidity of the samples, respectively such as viscosity and dielectric of the media. It is observed that Ω_2 and Ω_6 parameters are minimum at $x=5$ mol%

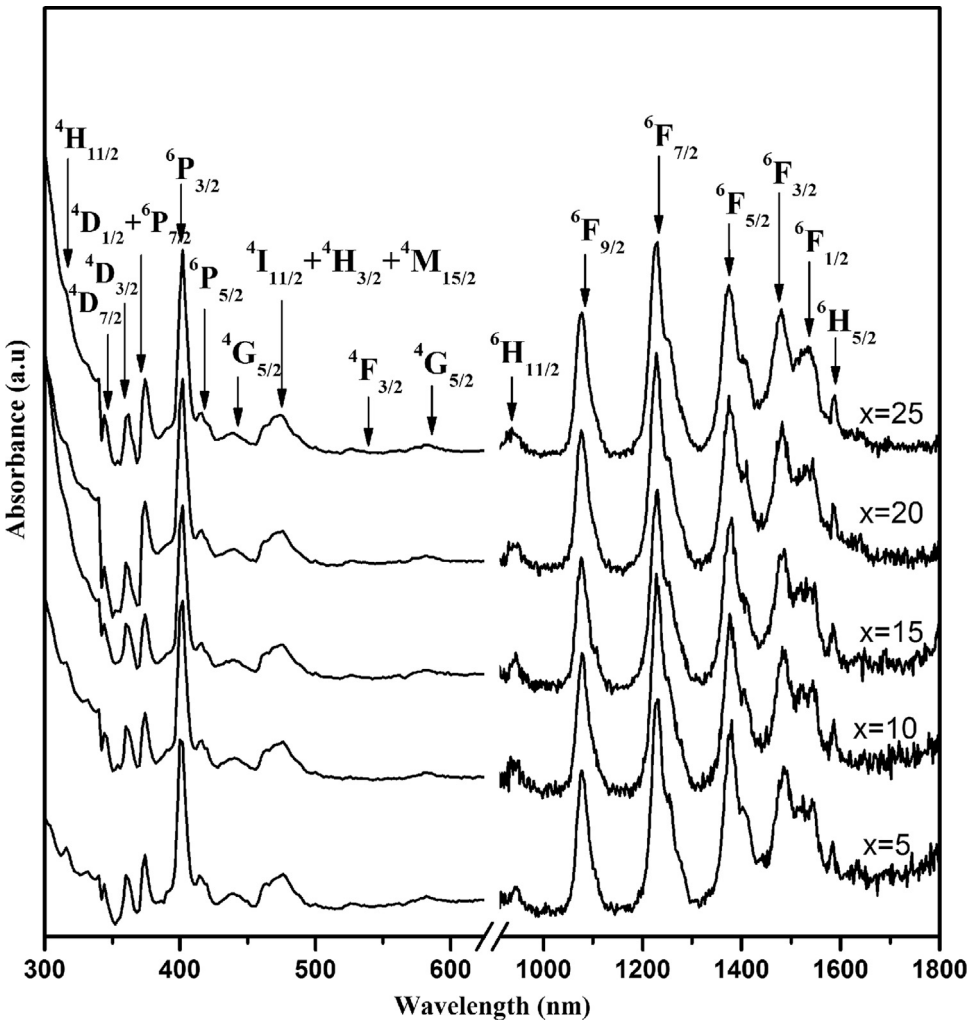

Fig. 3. Optical absorption spectra of Sm^{3+} doped zinc-phosphate glasses.

Table 2
Experimental and calculated spectral intensities ($f_{exp} \times 10^6$) of certain excited states and Judd–Ofelt intensity parameters (Ω_2, Ω_4 and Ω_6)($\times 10^{-20}$ cm^2) of certain excited states of Sm^{3+} doped zinc phosphate glass matrices.

S. no.	Transitions	5 mol%		10 mol%		15 mol%		20 mol%		25 mol%		$PbO–PbF_2$ [42]	Calibo [43]	ZBS [20]	LBTAF [44]
		f_{exp}	f_{cal}	f_{exp}	f_{cal}	f_{exp}	f_{cal}	f_{exp}	f_{cal}	f_{exp}	f_{cal}				
1	$^4P_{3/2}$	0.40	0.62	0.28	0.48	0.10	0.64	0.11	0.63	0.75	0.59				
2	$^4H_{11/2}$	1.05	–	1.64	–	0.87	–	6.19	–	2.27	–				
3	$^4D_{7/2}$	0.22	1.39	0.56	1.59	0.31	1.58	0.46	1.55	0.18	1.66				
4	$^4D_{3/2}$	1.69	1.00	1.57	0.78	2.04	1.03	1.67	1.01	1.99	0.95				
5	$^4D_{1/2}+^6P_{7/2}$	2.05	2.29	1.83	2.61	2.09	2.60	3.16	2.55	3.30	2.73				
6	$^6P_{3/2}$	6.74	5.86	6.57	4.59	6.81	6.06	6.91	5.94	6.90	5.61				
7	$^6P_{5/2}$	0.45	0.83	0.36	0.65	0.39	0.86	0.34	0.84	0.34	0.80				
8	$^4G_{9/2}$	0.74	0.11	0.78	0.11	0.72	0.12	0.60	0.12	0.40	0.12				
9	$^4I_{11/2}+^4I_{13/2}+^4M_{15/2}$	3.08	–	2.72	2.10	3.14	2.11	3.15	2.06	3.00	2.22				
10	$^4F_{3/2}$	0.09	1.85	–	–	0.08	–	0.13	–	0.13	–				
11	$^4G_{5/2}$	0.26	0.25	0.24	0.02	0.44	0.02	0.33	0.02	0.24	0.02				
12	$^6H_{11/2}$	0.30	0.69	0.42	0.80	0.39	0.79	0.44	0.78	0.41	0.83				
14	$^6F_{9/2}$	3.95	4.26	4.52	4.81	4.58	4.84	4.08	4.74	4.40	5.06				
15	$^6F_{7/2}$	6.00	6.06	6.46	6.39	6.68	6.75	6.79	6.63	7.15	6.92				
16	$^6F_{5/2}$	3.32	3.07	2.49	2.45	3.44	3.21	3.20	3.15	3.08	3.06				
17	$^6F_{3/2}$	1.34	1.75	1.47	1.58	1.57	1.95	1.56	1.88	1.97	2.10				
18	$^6F_{1/2}$	0.82	0.56	0.78	0.71	1.00	0.76	0.91	0.69	1.16	1.07				
19	$^6H_{15/2}$	0.11	0.03	0.12	0.04	0.10	0.04	0.10	0.04	0.11	0.04				
rms deviation		±0.64		±0.76		±0.68		±0.66		±0.66					
Ω_2		1.65		2.08		2.24		2.03		3.12		1.16	0.97	1.16	1.16
Ω_4		5.29		4.13		5.46		5.36		5.07		2.60	5.04	2.60	2.60
Ω_6		4.61		5.33		5.28		5.16		5.56		1.40	4.73	1.40	1.40

indicating lower covalency of Sm–O bond and lower rigidity of the glass matrix at $x=5$ mol%. These are maximum at $x=25$ mol% indicating higher covalency of Sm–O bond and higher rigidity of the glass matrix. The order of magnitude of Judd–Ofelt intensity parameters in all the glass systems is $\Omega_2<\Omega_6<\Omega_4$ except at $x=10$ mol% ($\Omega_2<\Omega_4<\Omega_6$) and 25 mol% ($\Omega_2<\Omega_4<\Omega_6$). Ω_λ can also be written as [31]

$$\Omega_\lambda = (2\lambda+1)\sum_{s,p}\left|A_{s,p}\right|^2 \Xi^2(s,\lambda)(2s+1)^{-1}, \quad \lambda = 2, 4, 6 \tag{3}$$

where $A_{s,p}$ are the crystal field parameters of rank s and are related to the structure around rare earth ions. $\Xi(s,\lambda)$ is related to the matrix elements between the two radial wave functions of 4f and the admixing levels e.g. 5d, 4f and the energy difference between these levels. It has been suggested by Reisfeld [37] that Ξ correlates to the nephelauxetic parameter β, which indicates the degree of covalency of the RE–O bond.

The position and intensity of certain electric dipole transitions of rare earth ions are very sensitive to the environment of the rare earth ion and they will obey the selection rules $|\Delta L|\le 2$, $|\Delta J|\le 2$ and $|\Delta J|=0$ such transitions are called as hypersensitive transitions [37]. For Sm^{3+} ion, the hypersensitive band, $^6H_{5/2}\rightarrow{}^6F_{1/2}$, $^6F_{3/2}$ clearly shows two peaks corresponding to two transitions $^6H_{5/2}\rightarrow{}^6F_{1/2}$ and $^6H_{5/2}\rightarrow{}^6F_{3/2}$. Hypersensitive of transition has been shown to be proportional to nephelauxetic ratio, β which indicates the covalency of RE–O bonds [37]. In the present work, the sum of the spectral intensities of the two hypersensitive transitions are 2.16, 2.25, 2.57, 2.47 and 3.13 and Ω_2 parameters are 1.65, 2.08, 2.24, 2.03 and 3.12 for $x=5$, 10, 15, 20 and 25 mol%, respectively. It is observed that the Ω_2 parameter decrease/increase with the decrease/increase of the sum of the spectral intensities of the two hypersensitive transitions of Sm^{3+} doped zinc-phosphate glasses. The spectral intensity of hypersensitive band is more at $x=25$ mol% of zinc-phosphate glass indicating high asymmetry of the crystal field around rare earth ions at this glass matrix. The shift of peak wavelength of the hypersensitive transition towards shorter wavelength with the increase of x in the glass matrix (because of nephelauxtic effect [37]) indicates decrease in covalency of RE–O bond. In the present work, the peak wavelengths of the hypersensitive transition are the same for different x values except at $x=25$ mol%. The peak wavelengths of the hypersensitive transition are 1544, 1544, 1544, 1544 and 1535 nm for $x=5$, 10, 15, 20 and 25 mol%, respectively.

The radiative transition probabilities (A), radiative lifetimes (τ) of certain excited states and branching ratios (β) of certain transitions are estimated by using Judd–Ofelt parameters Ω_λ ($\lambda=2$, 4,6) values thus obtained from absorption spectra. The radiative transition probability, $A_{rad}(aJ, bJ')$ for emission from an initial state aJ to a final ground state bJ' is given by Peacock [38]

$$A_{rad}(aJ, bJ') = \frac{64\pi^4}{3\lambda^3 hc^3(2J+1)}\frac{n(n^2+2)^2}{9} \sum_{\lambda=2,4,6}\Omega_\lambda\left|\left\langle SLJ\|U^\lambda\|S'L'J'\right\rangle\right|^2 \tag{4}$$

The total radiative transition probability, $A_T(aJ)$ involving all the intermediate terms between aJ and bJ' is given by the sum of the $A_{rad}(aJ, bJ')$ terms calculated over all terminal states bJ'

$$A_T(aJ) = \sum_{bJ'} A_{rad}(aJ, bJ') \tag{5}$$

The radiative lifetime, τ_R of the emission state is

$$\tau_R = \frac{1}{A_T(aJ)} \tag{6}$$

Table 3
Radiative lifetimes (τ_{rad}) (μs) of certain excited states of Sm^{3+} doped zinc-phosphate glasses.

S. no.	Transition	5 mol%	10 mol%	15 mol%	20 mol%	25 mol%
1	$^4G_{5/2}$	2498	2669	2289	2343	2254
2	$^6F_{11/2}$	666	626	595	606	576
3	$^6F_{9/2}$	745	719	668	679	650
4	$^6F_{7/2}$	988	971	888	902	854
5	$^6F_{5/2}$	1414	1444	1274	1298	1207
6	$^6F_{3/2}$	1923	2006	1721	1760	1577
7	$^6F_{1/2}$	2355	2437	2071	2160	1832

The fluorescence branching ratios, β of the emission transition is defined as

$$\beta(aJ, bJ') = \frac{A(aJ, bJ')}{A_T(aJ)} \tag{7}$$

The estimated radiative lifetimes of the excited states, $^4G_{5/2}$, $^6F_{11/2}$, $^6F_{9/2}$, $^6F_{7/2}$, $^6F_{5/2}$, $^6F_{3/2}$ and $^6F_{1/2}$ of Sm^{3+} doped zinc-phosphate glass samples are presented in Table 3. It is observed that for all zinc-phosphate glass matrices, the order of magnitude of τ_R parameter is $^4G_{5/2}>{}^6F_{1/2}>{}^6F_{3/2}>{}^6F_{5/2}>{}^6F_{7/2}>{}^6F_{9/2}>{}^6F_{11/2}$. Among the five glass matrices, the radiative lifetimes of all the excited states of Sm^{3+} are lower and higher at $x=25$ mol% and 5 mol%. The radiative lifetimes depend on the radiative transition probability and it is not affected by the phonon energy of the host. Fig. 4 shows the variation of A_T with the variation of x in Sm^{3+} doped zinc-phosphate glass matrices. The magnitude of branching ratios (β) of the four emission transitions, $^4G_{5/2}\rightarrow{}^6H_{5/2}$, $^6G_{5/2}\rightarrow{}^6H_{7/2}$, $^4G_{5/2}\rightarrow{}^6H_{9/2}$ and $^4G_{5/2}\rightarrow{}^6H_{11/2}$ of Sm^{3+} doped zinc-phosphate glass matrices are estimated. For these transitions, the branching ratio values are in the range 0.216–0.237, 0.375–0.396, 0.230–0.261, 0.090–0.098 respectively. Table 4 shows electric

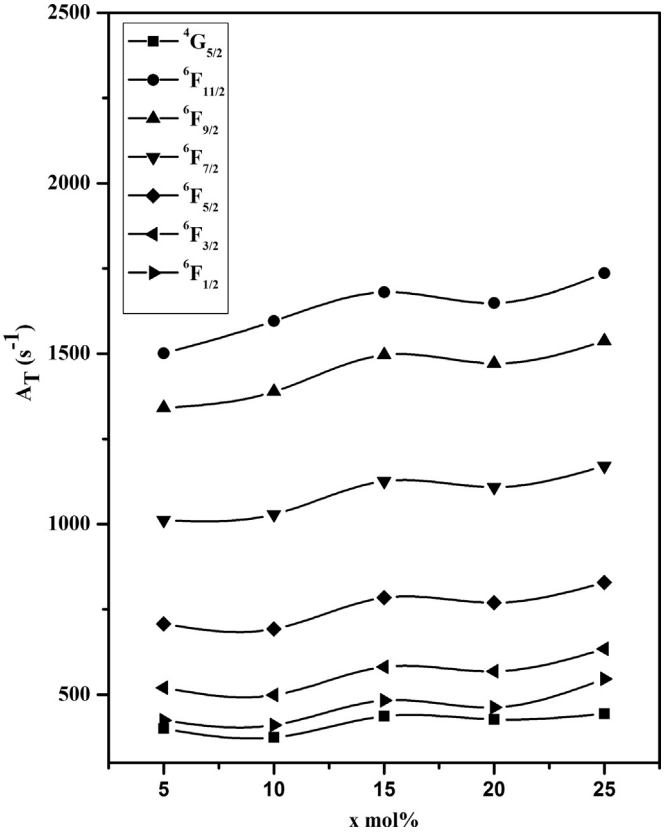

Fig. 4. Variation of AT with x in Sm^{3+} doped zinc-phosphate glasses.

Table 4
Energy of the transitions (ν) (cm^{-1}), electric dipole linestrengths ($S_{ed} \times 10^{-22}/e^2$) ($cm^2$), radiative transition probabilities (A_{red}) (s^{-1}), branching ratios (β) of $^4G_{5/2}$ level of Sm^{3+} in zinc-phosphate glass matrix (x=5 mol%).

SLJ→S′L′J′	ν	S_{ed}	A_{rad}	β
$^4G_{5/2}\rightarrow{}^6F_{11/2}$	6585	0	0	0
$^4G_{5/2}\rightarrow{}^6F_{9/2}$	7903	0.46	1.1	0.003
$^4G_{5/2}\rightarrow{}^6F_{7/2}$	9059	0.84	3.1	0.008
$^4G_{5/2}\rightarrow{}^6F_{5/2}$	9937	1.76	8.5	0.021
$^4G_{5/2}\rightarrow{}^6F_{3/2}$	10,460	0.17	1	0.002
$^4G_{5/2}\rightarrow{}^6F_{1/2}$	10,714	0	0	0
$^4G_{5/2}\rightarrow{}^6H_{15/2}$	10,877	0	0	0
$^4G_{5/2}\rightarrow{}^6H_{13/2}$	11,982	0.65	5.5	0.014
$^4G_{5/2}\rightarrow{}^6H_{11/2}$	13,520	3.21	39.2	0.098
$^4G_{5/2}\rightarrow{}^6H_{9/2}$	14,846	5.69	92	0.23
$^4G_{5/2}\rightarrow{}^6H_{7/2}$	16,052	7.58	155	0.387
$^4G_{5/2}\rightarrow{}^6H_{5/2}$	17,086	3.85	94.9	0.237

Total radiative transition probability A_T=400.3 s^{-1}, radiative lifetimes τ_R= 2498.13 μs.

dipole line strengths (S_{ed}), radiative transition properties (A_{rad}) and branching ratios (β) of some emission states of Sm^{3+} doped zinc-phosphate glass matrices (x=5 mol%).

3.4. Emission spectra and emission cross-section

The emission spectra of Sm^{3+} doped zinc phosphate glass matrices recorded at room temperature in the wavelength region 500–700 nm under the excitation wavelength 400 nm are shown in Fig. 5. The emission spectra have exhibited four transitions, which are assigned to $^4G_{5/2}\rightarrow{}^6H_{5/2}$ (564 nm), $^4G_{5/2}\rightarrow{}^6H_{7/2}$ (600 nm), $^4G_{5/2}\rightarrow{}^6H_{9/2}$ (646 nm) and $^4G_{5/2}\rightarrow{}^6H_{11/2}$ (703 nm). The spectral profiles of these emission bands are similar except in their full width at half maxima (FWHM) for all zinc-phosphate glass samples studied. The transition $^4G_{5/2}\rightarrow{}^6H_{7/2}$ with $\Delta J=\pm 1$ is a magnetic dipole (MD) allowed one but it is also electric dipole (ED) dominated, the other transition $^4G_{5/2}\rightarrow{}^6H_{9/2}$ is purely electric dipole (ED) one [39]. Generally, the intensity ratio of ED to MD transitions has been used to measure the symmetry of the local environment of the trivalent 4f ions. The greater the intensity of the ED transition, more dominant the asymmetry nature [34]. In the present work, it is observed that the emission transition, $^4G_{5/2}\rightarrow{}^6H_{5/2}$ (MD) of Sm^{3+} ions is more intense than $^4G_{5/2}\rightarrow{}^6H_{9/2}$ (ED) transition specifying the symmetric nature of the glass host. The emission intensities of the four transitions decreased as the

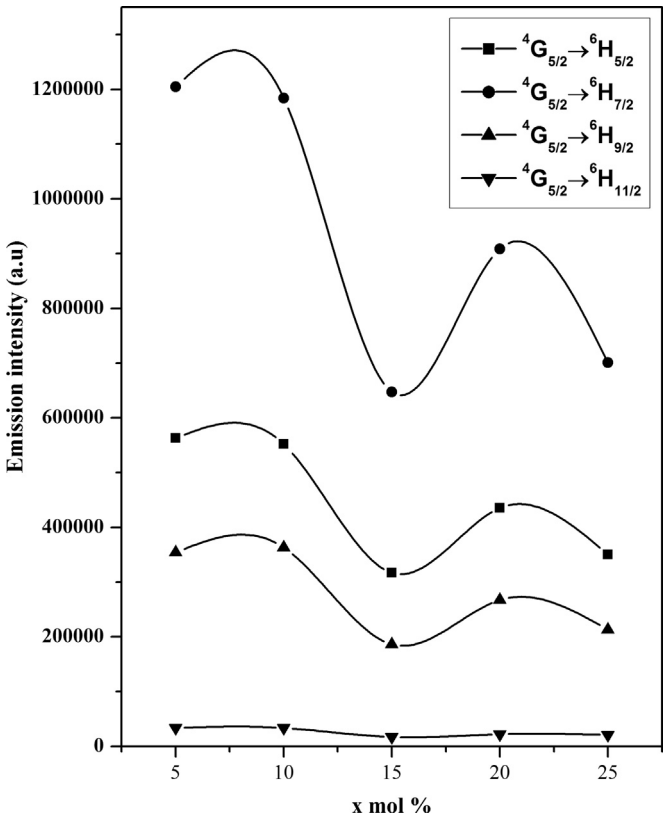

Fig. 6. Variation of emission intensity with x in Sm^{3+} doped zinc-phosphate glasses.

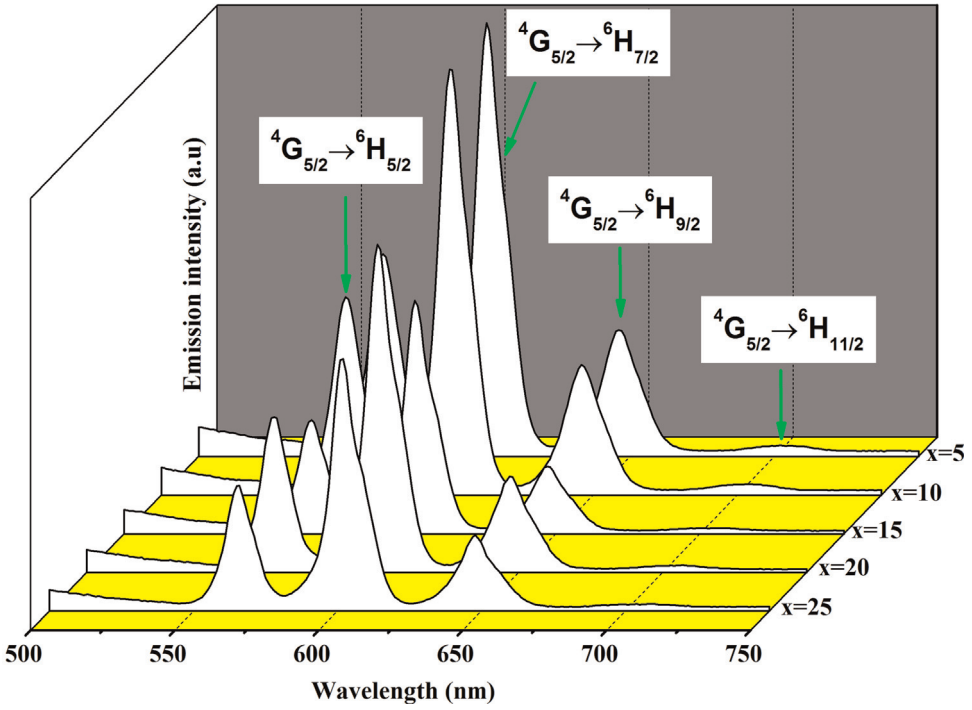

Fig. 5. Luminescence spectra of Sm^{3+} doped zinc-phosphate glasses. (λ_{exc}=400 nm).

Table 5
Radiative transition probabilities (A_{rad}), stimulated emission cross-sections (σ_p) and branching ratios (β_{exp} and β_{cal}) for emission transitions of Sm^{3+} doped zinc-phosphate glasses.

S. no.	Glass (mol%)	$^4G_{5/2} \rightarrow {}^6H_{5/2}$				$^4G_{5/2} \rightarrow {}^6H_{7/2}$				$^4G_{5/2} \rightarrow {}^6H_{9/2}$				$^4G_{5/2} \rightarrow {}^6H_{11/2}$			
		A_{rad} (s^{-1})	σ_p (10^{-21} cm^2)	β_{exp}	β_{cal}	A_{rad} (s^{-1})	σ_p (10^{-21} cm^2)	β_{exp}	β_{cal}	A_{rad} (s^{-1})	σ_p (10^{-21} cm^2)	β_{exp}	β_{cal}	A_{rad} (s^{-1})	σ_p (10^{-21} cm^2)	β_{exp}	β_{cal}
1	$x=5$	95	0.443	0.23	0.24	155	0.804	0.57	0.39	92	0.527	0.19	0.23	39	0.396	0.01	0.10
2	$x=10$	82	0.189	0.22	0.22	148	0.379	0.57	0.40	90	0.278	0.20	0.23	35	0.154	0.01	0.10
3	$x=15$	100	0.246	0.23	0.23	167	0.478	0.56	0.38	105	0.314	0.21	0.23	42	0.216	0.01	0.10
4	$x=20$	99	0.464	0.22	0.23	165	0.849	0.58	0.39	101	0.637	0.18	0.24	41	0.389	0.01	0.09
5	$x=25$	96	0.498	0.22	0.22	166	0.911	0.57	0.38	115	0.710	0.20	0.26	40	0.324	0.01	0.09

ZnO content increased from $x=5$ mol% to 15 mol%, but for 20 mol% of ZnO there is a slight increase in the emission intensity is observed. While for 25 mol% a sudden fall in intensity is noticed when compared to all the ZnO contents studied. Variation of four emission intensities of four peaks with x is shown in Fig. 6. It is known that intrinsic structure defects such as anion vacancies and non-bridging oxygen in phosphate glasses lowers the energy transfer efficiency from the host glass to the emission centers which lowers the emitted light [40]. The peak stimulated emission cross-section (σ) is obtained from [38]

$$\sigma_p = \frac{\lambda_p^4}{8\pi c n^2 \Delta\lambda_{eff}} A_{rad} \tag{8}$$

where λ_p is the peak wavelength and $\Delta\lambda_{eff}$ is the effective line width of the emission band. Due to asymmetry of the fluorescence bands, the effective line width was determined by integrating fluorescence spectral intensity divided by peak intensity. The evaluated peak stimulated cross-sections (σ_p) for the four transitions are presented in Table 5. Among four transitions, $^4G_{5/2} \rightarrow {}^6H_{7/2}$ transition found to have higher emission cross-section for all zinc-phosphate glass matrices. It is observed that at $x=25$ mol% glass shows higher emission cross-section and at $x=10$ mol% glass matrices shows lower emission cross-section for the four transitions. From the emission spectra, the branching ratios are determined by measuring the area of the corresponding emission band and dividing by the total integrated area of all the emission bands. These experimental and calculated (from the Judd–Ofelt method) branching ratios (β) are presented in Table 5.

3.5. Fluorescence decay lifetime measurement

The decay profiles of the fluorescence from the $^4G_{5/2}$ level of Sm^{3+} doped zinc phosphate glasses has been measured at room temperature under the excitation wavelength of 400 nm. The experimental lifetimes are estimated by taking the first e-folding times of the decay profiles. It is interesting to note that the decay traces are non-exponential behavior which may be due to higher concentration of Sm^{3+} ions (1 mol%). The nature of non-exponential behavior of Sm^{3+} doped zinc phosphate glasses can be analyzed by fitting to the Inokuti–Hirayama (IH) model [41]. According to IH model, the fluorescence decay intensity (I) is given by

$$I(t) = I_0 \exp\left\{-\frac{t}{\tau_0} - Q\left(\frac{t}{\tau_0}\right)^{3/S}\right\} \tag{9}$$

where t is the time after excitation, τ_0 is the intrinsic decay time of the donors in the absence of acceptors. The value of S ($=6$, 8 or 10) depends on whether the dominant mechanism of the interaction is dipole–dipole, dipole–quadrupole or quadrupole–quadrupole, respectively. The energy transfer parameter Q is defined as

$$Q = \frac{4\pi}{3}\Gamma\left(1 - \frac{3}{S}\right) N_0 R_0^3 \tag{10}$$

As can be seen from Eq. (10), Q depends on type of the mechanism S and the concentration of acceptors N_0, which is almost equal to the total concentration of lanthanide ions, and R_0 is the critical distance defined as a donor–acceptor separation for which the rate of energy transfer to the acceptors is equal to the rate of intrinsic decay of the donor.

In the present work, the decay curves are fitted to Eq. (9) for $S=6$ and are shown in Fig. 7 for all zinc phosphate glasses, respectively, indicating that the dominant interaction for energy transfer through cross-relaxation of Sm^{3+} ions is of dipole–dipole type. The possible energy transfer processes among the excited Sm^{3+} ions through cross relaxation channels are shown in Fig. 8.

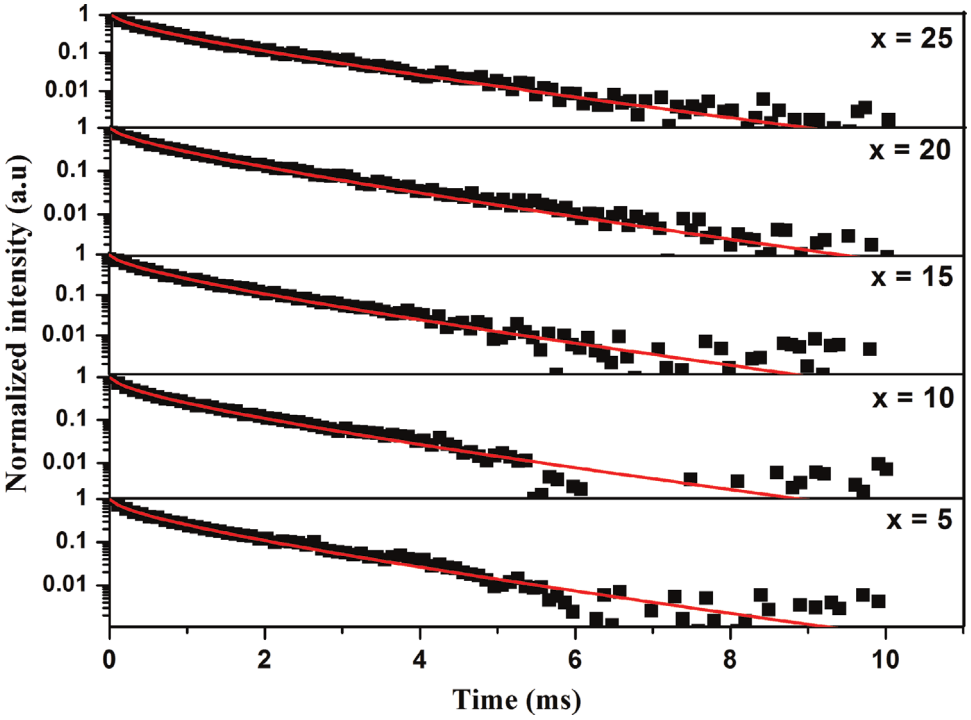

Fig. 7. Decay profiles of Sm^{3+} doped zinc phosphate glasses. (λ_{exc}=400 nm).

The magnitude of measured lifetimes (τ_{exp}) and energy transfer parameters (Q) from the analysis of non-exponential decay curves decreased with the increased concentration of ZnO (10–25 mol%) in phosphate glasses (shown in Fig. 9), indicating that τ_{exp} and Q are strongly dependent on glass composition even though concentration of Sm^{3+} is higher. The measured lifetime (τ_{exp}) can be expressed as [39]

$$\frac{1}{\tau_{\exp}} = \frac{1}{\tau_{rad}} + W_{MPR} + W_{ET} \tag{11}$$

where τ_{exp} and τ_{rad} are experimental and calculated radiative lifetime (resulting from Judd–Ofelt theory) W_{MPR} is the rate of multiphonon relaxation, W_{ET} is rate of energy transfer. But in case of Sm^{3+} ions, multiphonon relaxation (MPR) is negligible as there is a large energy gap of around 7000 cm^{-1} between the fluorescent level $^4G_{5/2}$ and next lower level. Hence, in the present work, the energy transfer process among the excited Sm^{3+} ions through cross relaxation channels is more prominent which also confirm from the shortening of the emission lifetime and discrepancy in between experimental (see Table 3) and calculated lifetimes.

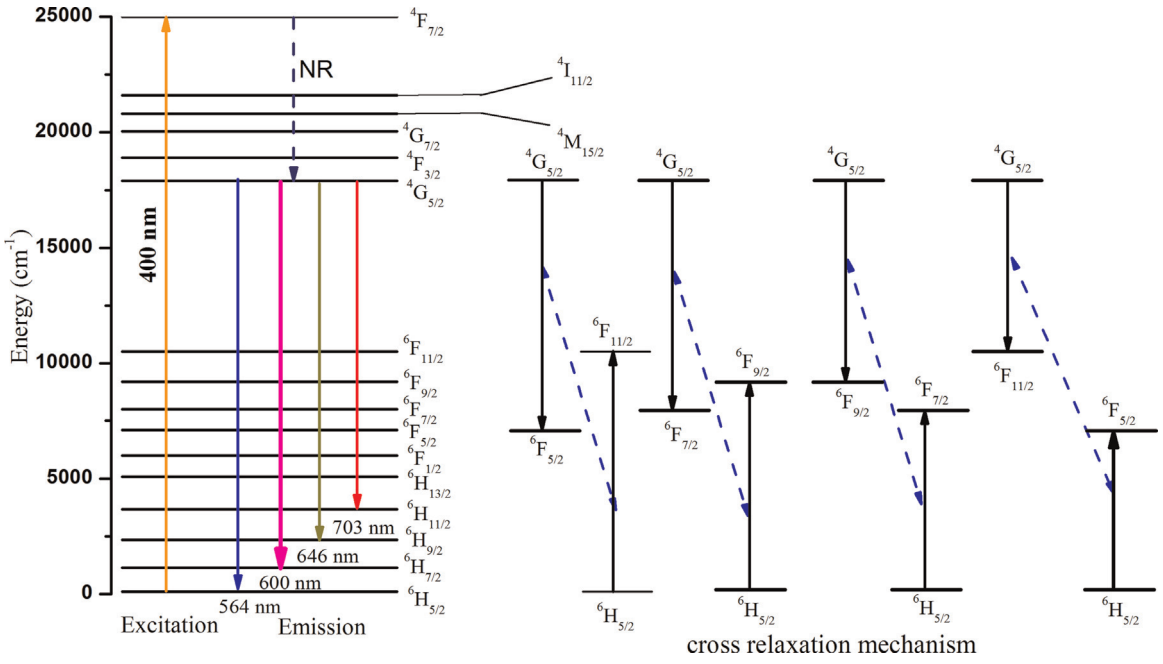

Fig. 8. Partial energy level diagram of Sm^{3+} showing excitation, emission and cross relaxation channels in zinc-phosphate glass.

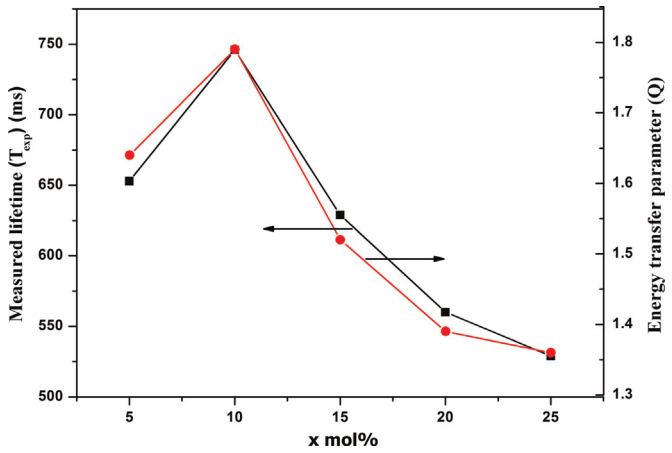

Fig. 9. Variation of measured lifetimes (τ_{exp}) and energy transfer parameter (Q) with x in Sm^{3+} doped zinc-phosphate glasses.

4. Conclusion

In summary, the Sm^{3+} doped zinc-phosphate glass matrices are prepared by using conventional melt-quench method. These glass samples were characterized by XRD, Raman, optical absorption, luminescence and emission decay lifetime measurements. The XRD patterns confirm the amorphous nature of prepared glass samples and Raman measurements reveals a network structure of phosphate units. The spectral intensities of the observed absorption bands have been calculated by the application of Judd–Ofelt theory. The small value of δ_{rms} indicates good fitting between experimental and calculated spectral intensities. Judd–Ofelt intensity parameter, Ω_2 is maximum at $x=25$ mol% which suggest the strong covalency at this glass matrix. The hypersensitive band, $^6H_{5/2} \rightarrow {}^6F_{1/2}$, $^6F_{3/2}$ clearly resolve into two peaks by stark splitting in zinc-phosphate glasses and the peak wavelengths of the hypersensitive transition are the same for different x values except at $x=25$ mol%. Hence $A_{s;p}$ is alone responsible for the increase or decrease in Ω_2 parameter. Spontaneous radiative transitions probabilities (A), radiative lifetime (τ_R), branching ratios (β_{exp} and β_{cal}) and emission cross-sections (σ_P) are calculated and discussed. Radiative lifetimes of certain excited states of Sm^{3+} are lower at $x=25$ mol%. Among four emission transitions, $^4G_{5/2} \rightarrow {}^6H_{7/2}$ transition has higher branching ratio and emission cross-section at $x=25$ mol%. Hence, the zinc-phosphate glass matrix with $x=25$ mol% is more useful for laser excitation. The decay curves are found to be non-exponential behavior for 1.0 mol% of Sm^{3+} doped zinc-phosphate glasses is due to the non-radiative energy transfer among the excited Sm^{3+} ions.

Acknowledgments

The author Y.C. Rathnakaram would like to thank the University Grants Commission (UGC) (No. F.40-443/2011(SR)), Delhi for financial support and M. Radha is greatful to TWAS-CNPq (No. 190077/2013-1).

References

[1] A. Jha, B. Richards, G. Jose, T. Teddy-Fernandez, P. Joshi, X. Jiang, J. Lousteau, Prog. Mater. Sci. 57 (2012) 1426.
[2] R.C. Stoneman, L. Esterowitz, Opt. Lett. 15 (1990) 486.
[3] S.D. Jackson, Nat. Photon. 6 (2012) 423.
[4] P. Wang, Y.P. Wang, L.M. Tong, Light Sci. Appl. 2 (2013) e102.
[5] B.V. Harbuzaru, A. Corma, F. Rey, J.L. Jordá, D. Ananias, L.D. Carlos, Angew. Chem. Int. Ed. 48 (2009) 6476.
[6] Th. Forster, Ann. Phys. 2 (1948) 55.
[7] P.I. Paulose, G. Jose, V. Thomas, N.V. Unnikrishnan, M.K.R.J. Warrier, Phys. Chem. Solids 64 (2003) 841.
[8] B.C. Joshi, R. Lohani, Bimal Pande, Indian J. Pure Appl. Phys. 39 (2001) 443.
[9] B.J. Chen, L.F. Shen, E.Y.B. Pun, H. Lin, Opt. Express 20 (2012) 879.
[10] G. Lakshminarayana, R. Yang, J.R. Qiu, M.G. Brik, G.A. Kumar, I.V. Kityak, J. Phy. D: Appl. Phys. 42 (2009) 015414 (12 pp.).
[11] J. Zang, D.L. Yang, E.Y.B. Pun, H. Gong, H. Lin, J. Appl. Phys. 107 (2010) 123111.
[12] M. Elisa, B.A. Sava, I.C. Vasiliu, R.C.C. Monteiro, J.P. Veiga, L. Ghervase, J. Non-Cryst. Solids 369 (2013) 55.
[13] H. Song, T. Hayakawa, M. Nogami, J. Appl. Phys. 86 (1999) 5619.
[14] E. Malchukova, B. Boizot, G. Petite, D. Ghaleb, J. Non-Cryst. Solids 353 (2007) 2397.
[15] G.J. Park, T. Hayakawa, M. Nogami, J. Phys.: Condens. Matter 15 (2003) 1259.
[16] R.L. Fuller, D.S. McClure, Phys. Rev. B 43 (1991) 27.
[17] B.R. Judd, Phys. Rev. 127 (1962) 75.
[18] G.S. Ofelt, J. Chem. Phys. 37 (1962) 511.
[19] Ch. Srinivasa Rao, C.K. Jayasankar, Opt. Commun. 286 (2013) 204.
[20] A. Agarwal, I. Pal, S. Sanghi, M.P. Aggarwal, Opt. Mater. 32 (2009) 339.
[21] M. Seshadri, K. Venkata Rao, J.L. Rao, Y.C. Ratnakaram, J. Alloys Compd. 476 (2009) 263.
[22] U. Caldino, A. Speghini, S. Berneschi, M. Bettinelli, M. Brenci, S. Pelli, G.C. Righini, Opt. Mater. 34 (2012) 1067.
[23] D. Rajesh, A. Balakrishna, Y.C. Ratnakaram, Opt. Mater. 35 (2012) 108.
[24] E.A. Davis, N.F. Mott, Philos. Mag. 22 (1970) 903.
[25] G.R. Moridi, C.A. Hogarth, in: W.E. Spear (Ed.), Proceedings of the Seventh International Conference on Amorphous and Liquid Semiconductors, 1997, p. 688.
[26] K. Shimakawa, J. Non-Cryst. Solids 43 (1981) 229.
[27] H. Fares, I. Jlassi, H. Elhouichet, M. Férid, J. Non-Cryst. Solids 396–397 (2014) 1.
[28] I. Jlassi, H. Elhouichet, M. Ferid, J. Mater. Sci. 46 (2011) 806.
[29] A.S. Shawoosh, A.A. Kutub, J. Mater. Sci. 28 (1993) 50.
[30] G. Chen, S. Baccaro, R. Giorgi, A. Cecilia, E. Mihokova, M. Nikl, J. Non-Cryst. Solids 326–327 (2003) 339.
[31] K. Meyer, J. Non-Cryst. Solids 209 (1997) 227.
[32] B.N. Nelson, G.J. Exarhos, J. Chem. Phys. 71 (1979) 2739.
[33] B. Tischendorf, J.U. Otaigbe, J.W. Weinch, M. Pruski, B.C. Sales, J. Non-Cryst. Solids 282 (2001) 147.
[34] P.R. Ehrmann, J.H. Campbell, J. Am. Ceram. Soc. 85 (2002) 1061.
[35] M.B. Saisudha, J. Ramakrishna, Phys. Rev. B 53 (1996) 6186.
[36] S. Tanabe, J. Non-Cryst. Solids 259 (1999) 1.
[37] R. Reisfield, Struct. Bonding 22 (1975) 123.
[38] R.D. Peacock, Struct. Bonding 22 (1975) 83.
[39] S. Tanabe, T. Ohyagi, S. Todoroki, T. Hanada, N. Soga, J. Appl. Phys. 73 (1993) 8451.
[40] W. Stambouli, H. Elhouichet, B. Gelloz, M. Fe´rid, N. Koshida, J. Lumin. 132 (2012) 205.
[41] Ch Basavapoornima, C.K. Jayasankar, J. Lumin. 153 (2014) 233.
[42] P. Nachimuthu, R. Jagannathan, V. Nirmal Kumar, D. Narayana Rao, J. Non-Cryst. Solids 217 (1997) 215.
[43] P. Srivastava, S.B. Rai, D.K. Rai, Spectrochim. Acta A 60 (2004) 637.
[44] B.C. Jamalaiah, J. Suresh Kumar, A. Mohan Babu, T. Suhasini, L. Rama Moorthy, J. Lumin 129 (2009) 363.